2 Theoretical considerations

2.1 Electron-molecule interactions

2.1.1 Classification of scattering processes

In general, electron-molecule scattering processes can be divided into two classes: direct and resonant scattering. In direct scattering the transit time of the electron is short and the scattering effectivity (the cross section; see chapter 2.1.3 on page 9) changes only gradually with the energy of the electron. Direct scattering includes elastic and inelastic scattering:

$$\mathrm{ABC} + \mathrm{e}^-(\epsilon_1) \rightarrow \mathrm{ABC} + \mathrm{e}^-(\epsilon_2) \qquad \epsilon_1 \approx \epsilon_2 \tag{2.1}$$

$$\mathrm{ABC} + \mathrm{e}^-(\epsilon_1) \rightarrow \mathrm{ABC}^* + \mathrm{e}^-(\epsilon_2) \qquad \epsilon_1 > \epsilon_2 \tag{2.2}$$

If inelastic scattering takes place some kinetic energy is transferred to the molecule, either in translational or internal degrees of freedom. The transfer of translational energy or a direct vibrational and rotational excitation is very inefficient in non-polar molecules due to the low mass of the electron and the conservation of momentum. On the other hand electronic excitation is more efficient.
If the kinetic energy of the electron exceeds the ionisation energy of the molecule, ionisation may occur:

$$\mathrm{ABC} + \mathrm{e}^-(\epsilon) \rightarrow \mathrm{ABC}^{*+} + 2\mathrm{e}^- \qquad \epsilon > \mathrm{IE} \tag{2.3}$$

In these processes the electron serves primarily as projectile to provide the energy. The nature of the electron becomes more important at energies below the

ionisation threshold, when resonances occur. Resonances are characterised by sharp changes in cross sections with energy and transit times that are considerably longer than the normal duration for passing the molecule. For instance an electron having a kinetic energy of 2 eV takes 10^{-15} s (1 fs) to travel 10^{-9} m (1 nm). In contrast the resonance lifetime is usually longer than 1 fs. During this period an empty molecular orbital (MO) is occupied and hence a negative ion is formed:

$$\mathrm{ABC} + \mathrm{e}^-(\epsilon_1) \rightarrow \mathrm{ABC}^{\#-} \tag{2.4}$$

The generated anion is referred to as transient negative ion (TNI) [28] since it is usually unstable towards loss of the additional electron, termed as *autodetachment*:

$$\mathrm{ABC}^{\#-} \rightarrow \mathrm{ABC}^* + \mathrm{e}^-(\epsilon_2) \qquad \epsilon_1 > \epsilon_2 \tag{2.5}$$

The TNI may be generated in a vibrational excited state of the anion. If so the neutral can be left after autodetachment in an excited state and the detached electron has lost some energy corresponding to the vibrational energy. This energy loss process can occur in electron energy loss spectroscopy (EELS) to measure vibrational and electronic excitation of molecules. Resonant vibrational excitation can be observed in the excitation function for a particular vibration, in which the excitation cross section for a constant energy loss is recorded versus the incident electron energy.

The autodetachment-lifetime τ is determined by the energy width Γ of the negative ion state according to the Heisenberg uncertainty principle:

$$\tau \approx \frac{\hbar}{\Gamma}, \tag{2.6}$$

with $\hbar$ being the Planck constant ($\mathrm{h}/2\pi = 6.6\times10^{-16}$ eV·s). For a resonance having a lifetime of $\approx 10^{-14}$s the energy width thus is below 1 meV.

The TNI can be stabilised if the excess energy is released, e.g. by collisions with

adjacent molecules in a cluster or condensed environment [29]:

$$ABC^{*-} + AB \rightarrow ABC^{-} + ABC^{*} \tag{2.7}$$

A single anion (at single-collision conditions) is able to loose the extra energy only through radiative cooling which is usually much slower (10^{-9} s - 10^{-8} s for electronic excitation) than autodetachment:

$$ABC^{*-} \rightarrow ABC^{-} + h\nu. \tag{2.8}$$

Another process that competes with autodetachment is dissociation into a stable negative ion and one or more neutral radicals:

$$ABC^{\#-} \rightarrow AB + C^{-} \tag{2.9}$$

This process becomes efficient when the extra electron in the TNI occupies an MO with antibonding character. It is assigned as dissociative electron attachment (DEA) [28] and the work presented here investigates DEA mechanisms in biologically relevant molecules by means of free-electron attachment at defined energies and mass spectrometric detection of the anions.

2.1.2 Dissociative electron attachment (DEA)

The capture of an electron into a virtual orbital enables a bond rupture already at very low energy, if the binding energy of the extra electron (the electron affinity) is large enough to compensate the bond dissociation energy D(AB-C). The lowest energy limit for DEA - the thermodynamic threshold ΔH_0 - hence is given by:

$$\Delta H_0 = D(AB - C) - EA(C), \tag{2.10}$$

with EA(C) being the electron affinity of C. The actual appearance energy AE of the fragment anion C^{-} may be at a larger value than the thermodynamic threshold resulting in excess energy E* carried by the fragments:

$$AE = D(AB - C) - EA(C) + E^{*}, \tag{2.11}$$

The appearance energy is determined by the *vertical* attachment energy (VAE, see figure 2.3) of the molecule ABC, i.e. the vertical Franck-Condon transition to the anionic potential energy surface. The whole DEA process is displayed in figure 2.1 in a simplified two-dimensional potential energy diagram assuming that the Born-Oppenheimer approximation is valid. The anionic potential energy

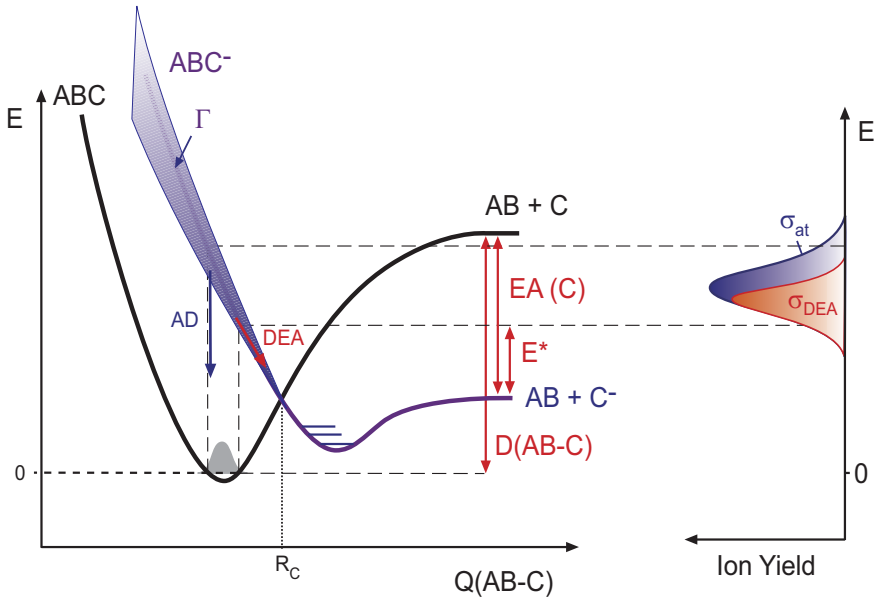

Figure 2.1: Born-Oppenheimer potential energy diagram.

curve shown in figure 2.1 is repulsive in the Franck-Condon region, thus the geometry of the TNI changes and one or more bonds get elongated. Until the crossing point R_C of neutral and anionic curve is reached, autodetachment is still possible according to the energy width of ABC^- (Γ) (equation 2.6). As Γ is smaller at larger bond distance (lower energy) dissociation is more likely at lower transition energies (in addition to the already enlarged bond and hence the shorter duration of dissociation), whereas autodetachment dominates at smaller bond distance (higher transition energies). If the anionic curve has a minimum, the parent ion ABC^- may be observed, if the excess energy can be released or redistributed into other vibrational degrees of freedom.

The ion yield curve shown on the right-hand side of figure 2.1 is determined by

the initial formation of the TNI and its shape represents in a first approximation the reflection of the ground state vibrational wave function of the neutral at the anionic potential [28]. This reflection principle does not include autodetachment, nonetheless the peak shape (i.e. width, slope and structures) contains information on the initial Franck-Condon transition and the relative positions of the anionic and neutral potential surfaces.

The dissociation reactions become more complicated in larger molecules when multiple bond breaking and forming occurs. As will be shown in the present work a scrambling of atoms can be observed already at low energies if thermodynamically stable products are generated:

$$\mathrm{ABC}^{\#-} \rightarrow \mathrm{AC} + \mathrm{B}^- \tag{2.12}$$

Under the present experimental conditions the fragment anions are detected much later ($\approx 10^{-5}\,\mathrm{s}$) than the time for dissociation of the TNI. Thus the observed ion B^- may also be a result of the dissociation of a metastable intermediate AB^-:

$$\mathrm{ABC}^{\#-} \rightarrow \mathrm{AB}^- + \mathrm{C} \rightarrow \mathrm{A} + \mathrm{B}^- + \mathrm{C} \tag{2.13}$$

In summary, the *energetic position* of a signal in the ion yield curve is determined by the vertical attachment energy (VAE), convoluted with the (energy dependent) probability for decomposition into the particular fragment ion, and the *intensity* of the signal is governed by the autodetachment rate and the Franck-Condon factor of the initial transition, that is the square of the overlap integral of the neutral ground state and the anionic wave function. The intensity is expressed as (energy dependent) cross section (see next section).

2.1.3 Cross sections

The effectivity of a DEA process can be expressed by the DEA cross section σ_{DEA}. In general a cross section gives the probability that a certain interaction

occurs. The total scattering cross section σ_T includes all scattering interactions like elastic scattering, excitation, ionisation and electron attachment:

$$\sigma_{\mathrm{T}} = \sigma_{\mathrm{el}} + \sigma_{\mathrm{ex}} + \sigma_{\mathrm{ion}} + \sigma_{\mathrm{at}}. \tag{2.14}$$

The DEA cross section σ_{DEA} and the cross section for electron attachment σ_{at} are connected by the probability P that the TNI dissociates:

$$\sigma_{\mathrm{DEA}} = \sigma_{\mathrm{at}} \cdot \mathrm{P}. \tag{2.15}$$

The TNI is able to dissociate if the extra electron is not autodetached until the dissociating system reaches R_C. Therefore P is referred to as survival probability and can be calculated from the time τ_{DEA} it takes the TNI to dissociate and the autodetachment lifetime τ_{AD}:

$$\sigma_{\mathrm{DEA}} = \sigma_{\mathrm{at}} \cdot \mathrm{e}^{-\frac{\tau_{\mathrm{DEA}}}{\tau_{\mathrm{AD}}}}, \tag{2.16}$$

The autodetachment lifetime τ_{AD} corresponds to the lifetime of the anionic electronic state and is given by equation 2.6. τ_{DEA} can be calculated from the radial velocity v(R') between the fragments:

$$\tau_{\mathrm{DEA}} = \int_{\mathrm{R}}^{\mathrm{R_C}} \frac{\mathrm{dR'}}{\mathrm{v(R')}}. \tag{2.17}$$

R is the bond distance from where the electronic transition takes place and R_C is the crossing point (see figure 2.1). An estimation of the dissociation time can be obtained by the vibrational period along which the dissociation occurs, which is usually tens of femtoseconds (fs).

The attachment cross section is connected with the rate constant k of the electron attachment reaction:

$$\mathrm{k} = \int_0^\infty \sigma_{\mathrm{at}} \mathrm{f(v)vdv}, \tag{2.18}$$

where f(v)dv denotes the Maxwell-Boltzmann velocity distribution of electrons $f(v)dv \propto v^2 exp(-mv^2/2kT)dv$. Taking the mean velocity $\bar{v}$ and mean cross section $\bar{\sigma}$ the rate constant can be approximated by:

$$\mathrm{k} = \bar{\sigma_{\mathrm{at}}} \bar{\mathrm{v}}. \tag{2.19}$$

k can be determined in swarm experiments, hence the mean cross section can be calculated using additionally the distribution function for electrons.

Low energy electrons have a large DeBroglie wavelength ($\lambda = h/(2mE)^{1/2}$), e.g. an electron of 1 eV kinetic energy has a wavelength of 1.2 nm, which is larger than the size of a small molecule. In quantum mechanics a beam of free electrons at defined energy can be represented by a plane wave. The plane waves are superpositions of partial waves with different angular momentum l, i.e. s-waves for l = 0 and and p-waves for l = 1. In resonance scattering one or more partial waves undergo constructive interference with the target, for instance s-waves „fit“ into the spherical LUMOs of CCl_4 or SF_6 and hence interfere constructively [30, 31]. The total scattering cross section for a spherically symmetric force field can be expressed as:

$$\sigma_{\mathrm{T}} = \frac{4\pi}{\mathrm{k}^2} \sum_{\mathrm{l}=0}^{\infty} (2\mathrm{l}+1)\sin^2\delta_{\mathrm{l}}, \tag{2.20}$$

with $k^2 = (2m\epsilon)/\hbar^2$, ϵ the electron energy, and δ_l is the phase shift of the electron wave before and after scattering. The extent of the phase shift is a measure of the strength of the interaction between the wave and the target. From equation 2.20 it is obvious that the total cross section rises at low energies, where only s-waves contribute, according to $\sigma_T \propto 1/\epsilon$. However, a closer inspection of the attachment cross section shows that at very low energies (< 10 meV) the cross section for s-wave attachment rises less strong according to $\sigma \propto \epsilon^{-\frac{1}{2}}$ [32, 33]. This was confirmed experimentally for SF_6 at energies below 1 meV [34]. p-wave attachment even drops down with $\sigma \propto \epsilon^{\frac{1}{2}}$ as was confirmed experimentally through DEA cross sections for Cl^- production subsequent to electron attachment to Cl_2 [35]. The threshold behaviour of the cross section is known as „Wigner threshold law“ [32].

2.1.4 Dynamics of anion formation

If the molecule possesses a positive electron affinity by definition a bound state exists for the extra electron. However, in free-electron attachment the captured electron has a positive energy and the anion is then formed energetically above the ground state of the anion. The ground state can only be reached by release or redistribution of the extra energy. In the vertical transition depicted in figure 2.3, the extra electron must be somehow trapped to prevent immediate autodetachment.

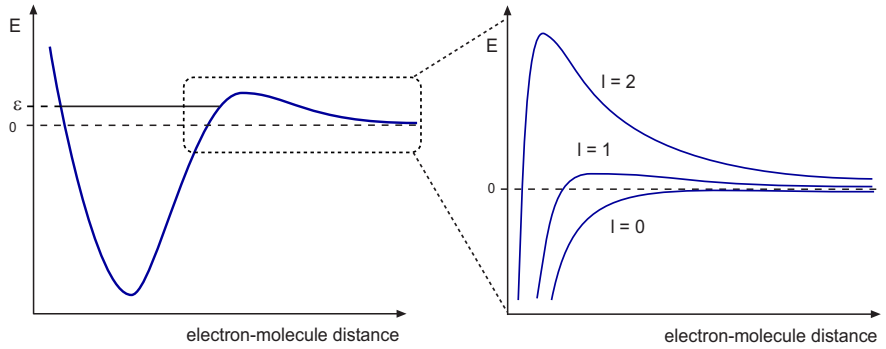

Figure 2.2: Effective potential of the electron-molecule interaction including the attractive polarization potential and the repulsive centrifugal potential. On the left side also the pauli repulsion is shown at small distances, the formation of the potential barrier is shown on the right for different values of the angular momentum l.

As the electron interacts with a neutral molecule the binding energy of the electron is weak. At larger distances the interaction can be approximated by a charge-induced dipole potential:

$$V_\alpha = -\frac{\alpha e^2}{2r^4}. \tag{2.21}$$

α denotes the polarizability of the molecule. Due to the angular momentum of the electron a repulsive centrifugal potential becomes important at shorter distances resulting in an effective potential of the following form:

$$V = V_l + V_\alpha = \frac{\hbar^2 l(l+1)}{2\mu r^2} - \frac{\alpha e^2}{2r^4}, \tag{2.22}$$

For l≠0 a centrifugal barrier is formed (figure 2.2), i.e. an electron can be attached into a vacant MO with suitable symmetry and is captured temporarily by the barrier. This is referred to as *shape* resonance [36, 37] (figure 2.3) as the trapping mechanism is determined by the shape of the effective potential (figure 2.2). In the picture of partial waves the electrons can be regarded as plane waves containing all components of angular momentum. An energetically accessible and empty MO that is characterised by a particular angular momentum l may be able to capture an electron having this particular symmetry. No further changes

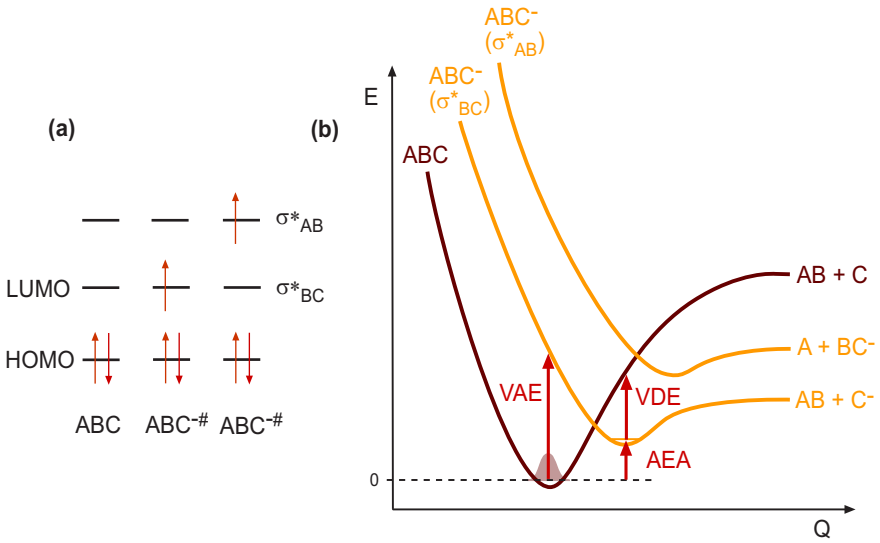

Figure 2.3: (a) Electronic configuration in a neutral molecule and in two kinds of $\sigma*$ shape resonances, (b) Schematic potential energy diagram showing the total energy of the neutral molecule ABC and two anionic states, the arrows indicate the vertical attachment energy (VAE), the adiabatic electron affinity (AEA) and the vertical detachment energy (VDE).

in electron configuration are involved and this kind of resonance hence is also referred to as *one particle* (1p) resonance. Shape resonances usually occur at energies below 4 eV and have short lifetimes (10^{-15} - 10^{-10} s [36]) since the electron can escape by tunneling through the barrier. Concerning LEE induced strand breaks in DNA, shape resonances are discussed to be involved in single strand breaks below 2 eV[8].

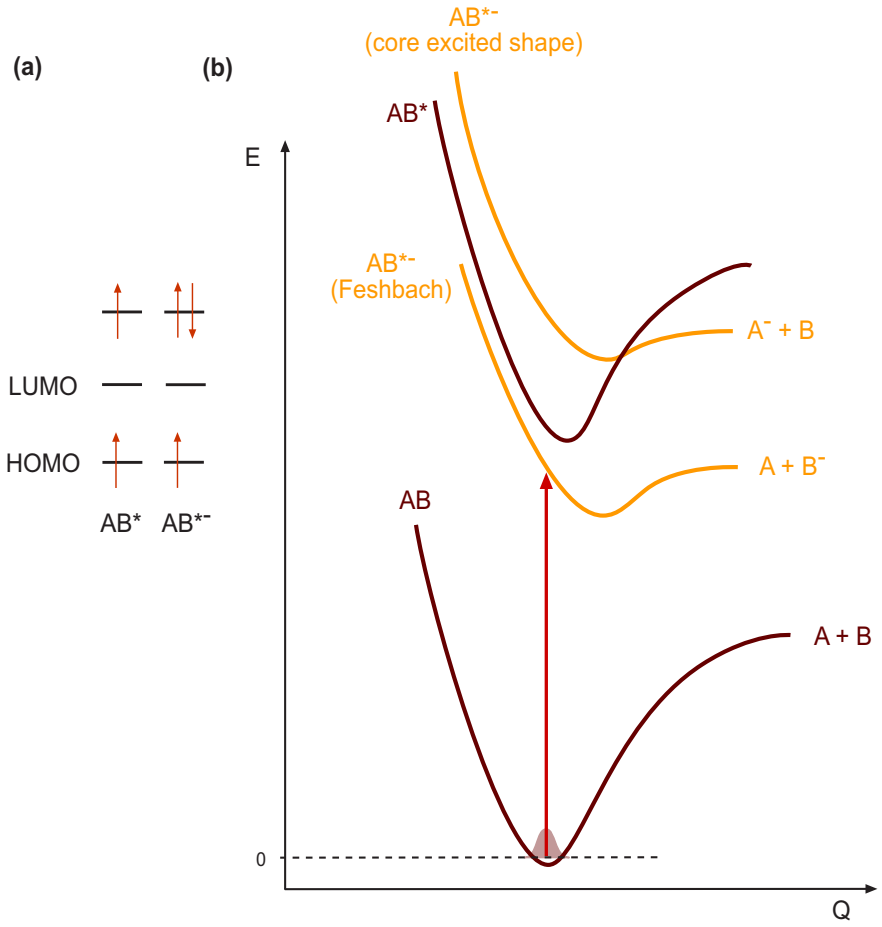

Figure 2.4: (a) Electronic configuration in an excited neutral molecule and core excited anion, the excitation may proceed into a valence (e.g. the LUMO) or a Rydberg type orbital. (b) Schematic potential energy diagram showing the total electronic energy of the neutral ground state and electronically excited molecule AB, and the core excited shape and Feshbach resonances.

If the energy of the incoming electron is large enough to induce electronic excitation in the neutral molecule, an anion is created with two electrons occupying normally empty MOs. This is a *core excited* or *two particle one hole* (2p-1h) resonance. The electronic excitation often involves valence orbitals leading usually to a TNI lying energetically above the excited neutral (the parent electronic state, see figure 2.4). This is also more specifically termed core excited shape resonance and it decays easily into its parent state. Core excited resonances occur at en-

ergies close to electronic excitation and are most likely involved in production of single and also double strand breaks in DNA around 10 eV [6, 7].
The electron affinity of the excited neutral may be positive and hence the generated TNI lies energetically below the parent excited state. In this case the lifetime of the anion is considerably longer as the parent excited state cannot be reached anymore. This is referred to as a *Feshbach* resonance (figure 2.4).

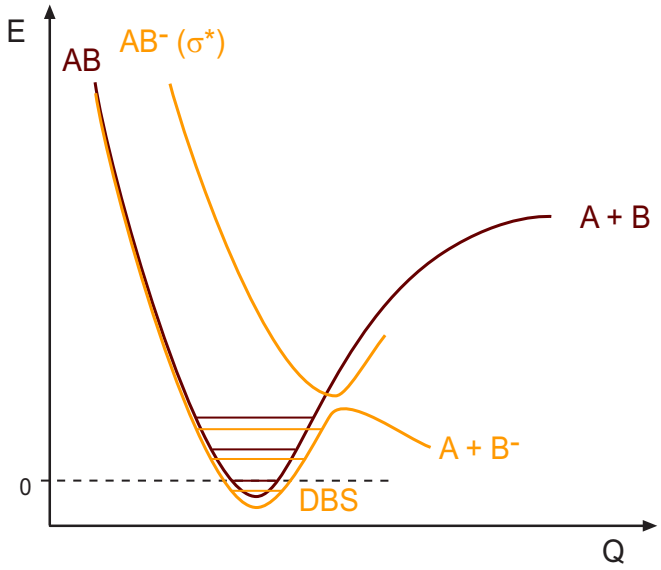

Figure 2.5: Formation of a dipole bound state (DBS). The vibrational levels of the DBS lie below the corresponding levels of the neutral, hence this is also referred to as vibrational Feshbach resonance (VFR).

At low energies *vibrational Feshbach* resonances can occur (figure 2.5) if the vibrational levels of the TNI lie below the corresponding states of the neutral [38]. This trapping mechanism is likely in molecules having large polarizability and a very large dipole moment ($> 2.5\,\mathrm{D}$) leading to a long-range attractive interaction. The extra electron becomes localised in a very diffuse Rydberg-type orbital on the positive site of the dipole resulting in an anion having similar geometry like the neutral. Hence the anionic state is also referred to as dipole bound state [39]. In free-electron attachment these states are only accessible if internal vibrational redistribution takes place to release the excess energy. A VFR may

serve as a doorway for dissociation at low energy if it is coupled to a dissociative valence state as it is shown schematically in figure 2.5. In this case a VFR can be observed in DEA as it was shown previously for example in N_2O [40], ethylene carbonate [41] and also in the nucleobases uracil [42] and thymine [43]. On the other hand these states can be probed by means of electron transfer from highly excited Rydberg atoms [39] where the binding energy of the transferred electron corresponds to the (positive) electron affinity of the molecule.

2.2 Fundamental processes in radiation damage

2.2.1 Radiation damage

The harmful character of radioactive radiation became apparent soon after its discovery by Becquerel in 1896. Some years later in 1927 the mutagenic effects of x-rays were first discovered by Muller [44], who was awarded with the Nobel prize in 1946. Depending on the dose (the energy deposited per unit mass[1]) the acute effects on the human body range from fatigue ($< 1\,\mathrm{Sv}$) over fever and epilation ($1\,\mathrm{Sv}$) up to the death ($> 4\,\mathrm{Sv}$). Long-term effects are an alteration of the genome possibly resulting in cancer. The biological effectiveness of radiation is characterised by the linear energy transfer (LET), that is the amount of energy deposited per length ($\mathrm{LET} = dE/dl$). Particle radiation like α particles possess the highest LET and high energy electromagnetic radiation like γ rays have a low LET.

However, this is a phenomenological description of radiation damage. The molecular mechanisms are a series of complex physical, chemical and biological events that are only partially understood. Therefore it is useful to divide the different processes according to their timescale after deposition of the initial radiation quantum as it is depicted in figure 2.6. The first processes after irradiation are ionisation and excitation of molecules proceeding within $10^{-15}\,\mathrm{s}$. In a subsequent cascade a large number of electrons and ions are produced (similar to equation 2.23) having enough energy to induce further ionisation events until the high initial energy is distributed to a large number of secondary particles. Secondary electrons get finally solvated after $10^{-12}\,\mathrm{s}$ [45] and are then chemically rather inactive [3]. However, before they are thermalised, electrons are highly reactive undergoing DEA usually within 10^{-14} - $10^{-10}\,\mathrm{s}$ (see chapter 2.1.2).

[1] The absorbed dose is measured in Gray: $1\,\mathrm{Gy} = 1\,\mathrm{J/kg}$, but does not reflect the different biological effects of the different types of radiation. The equivalent dose includes a weighing factor for the radiation and is measured in Sievert: $1\,\mathrm{Sv} = 1\,\mathrm{J/kg}$.

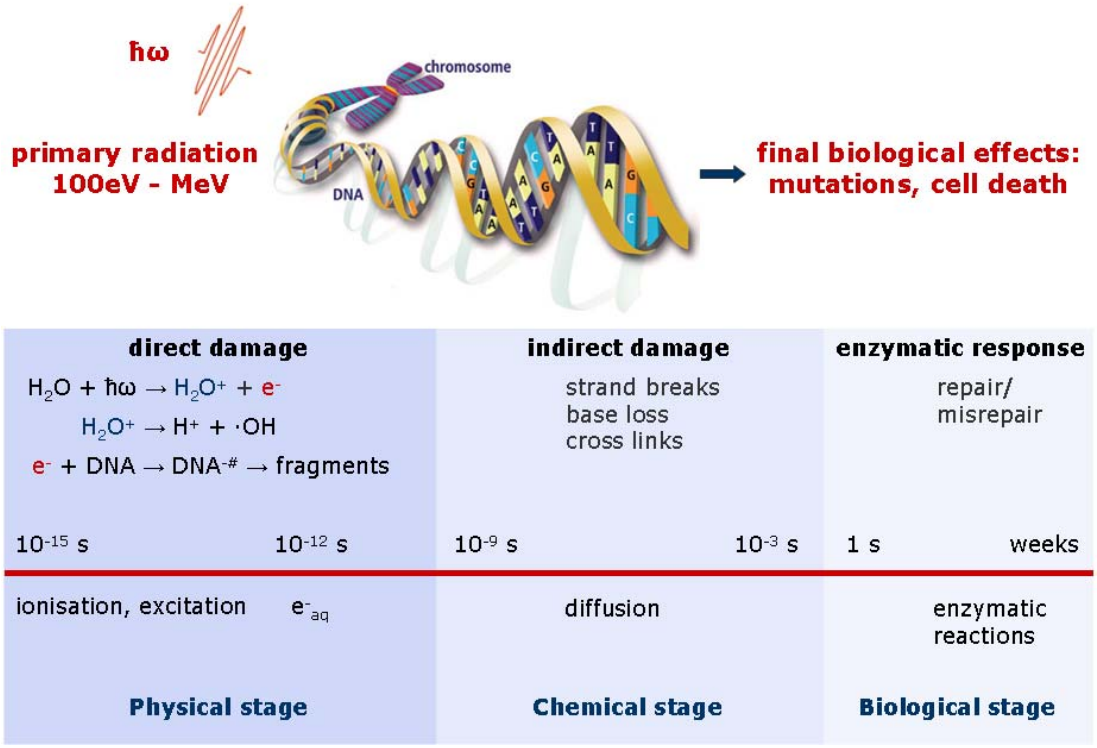

Figure 2.6: Outline of relevant processes in radiation damage, starting with the initial events of ionisation and excitation up to the biological effects of DNA damage. Dissociative electron attachment is crucial since it takes place very early in timescale.

About 80 % of the cell are composed of water and thus the interaction of photons with a cell leads to the formation of the OH radical - besides electrons and ions:

$$H_2O + h\nu \rightarrow H_2O^+ + e^- \tag{2.23}$$

$$H_2O^+ \rightarrow H^+ + OH \tag{2.24}$$

The high reactivity of the OH radical leads to further reactions with DNA resulting in strand breaks, base loss and base modifications [46]. The effects of the chemical stage (figure 2.6) are referred to as indirect damage.

The biological stage is characterised by enzymatic reactions that are aimed to repair the DNA damage and are initialised after a few seconds. Single strand breaks can be repaired using the other strand as a template. However, if the damage is not or incorrectly repaired a mutation results. Two strand breaks on

opposite sites can lead to a double strand break, which is very difficult to repair and thus has severe biological effects.

2.2.2 The role of electrons

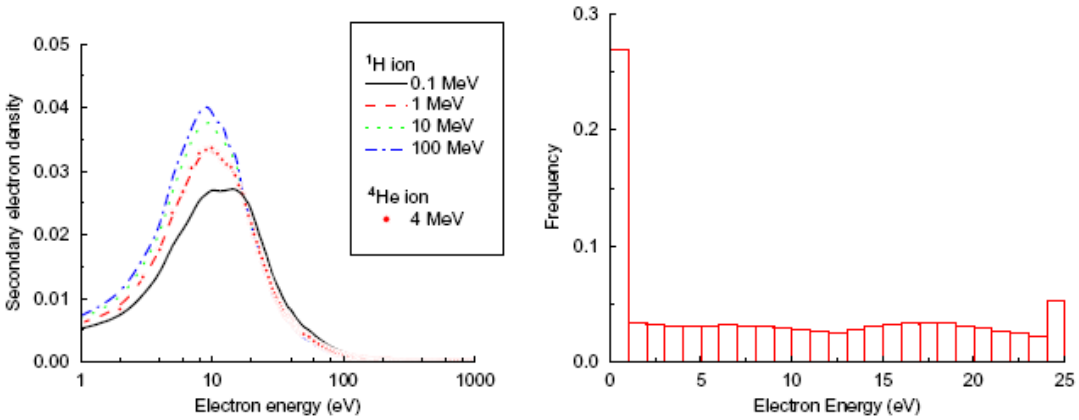

Figure 2.7: Energy distribution of secondary electrons produced in liquid water by (a) primary ionisation events caused by proton radiation of different energy; (b) 1 MeV primary electron irradiation taking all further interaction of energetic secondary electrons into account, thus representing the final energy distribution of secondary electrons. A fraction of about 27 % possess a kinetic energy between 0 and 1 eV. Taken from [5].

Figure 2.7 shows the energy distribution of secondary electrons that are produced in liquid water by high energy radiation according to very recent Monte-Carlo calculations [5]. The most probable energy of a secondary electron produced by the primary ionisation events is about 9 eV. If all further ionisation events are taken into account that are caused also by energetic secondary electrons one arrives at an electron energy distribution shown in figure 2.7 b, i.e., a large fraction (27 %) possesses a kinetic energy below 1 eV. More than 80 % of the primary energy from 1 MeV proton radiation is carried by low energy electrons after the primary ionisations [5].

In the traditional notion of radiation damage only photons and electrons with an energy exceeding the ionisation threshold of molecules were assumed to contribute

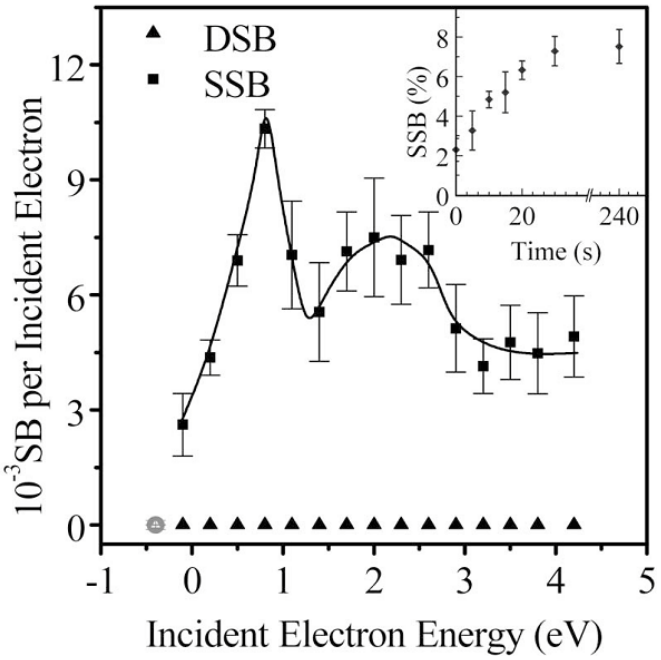

Figure 2.8: Energy dependence of low energy (0 - 4 eV) electron induced single strand breaks (SSBs) in plasmid DNA. SSBs occur already close to zero eV. Taken from [8].

to the damage. However, in the meantime it is well-known that electrons at energies below the ionisation threshold are able to induce effective decomposition of biomolecules via DEA. A direct comparison of the damage induced by x-ray photons and secondary electrons [47] reveals a more effective strand break yield by low energy electrons. Additionally DEA results in anionic and radical fragments that might further react with DNA. For instance, a frequently observed reaction in DEA to organic molecules is abstraction of an H radical that might further react with other targets, and a closed shell anion. The effectivity of DNA strand cleavage within the chemical stage is determined by the initial events of energy deposit and production of secondary particles. It is hence crucial to investigate low energy electron interaction with DNA and the surrounding molecules that occur at an early time of radiation damage.

The resonant behaviour that is observed for the SSB and DSB yield in condensed phase (shown in figures 2.8 and 2.9) exhibits a similar energy dependence like

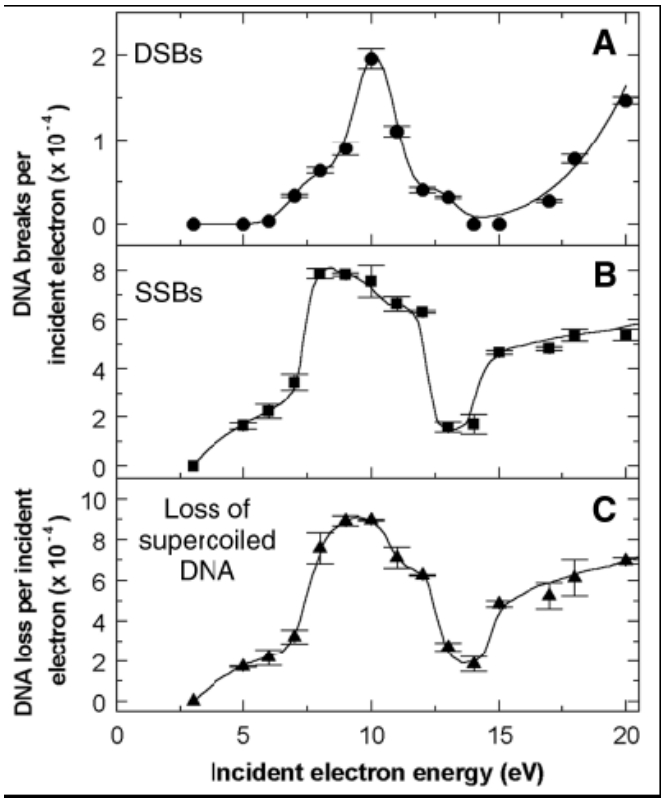

Figure 2.9: Yield of single, double and multiple strand breaks in plasmid DNA induced by low energy (3 - 20 eV) electrons. Note that the scale is lower than in figure 2.8. Taken from [6].

isolated DNA building blocks in the gas phase. All nucleobases (NB) undergo dissociative electron attachment within two resonance features at 0 - 4 eV and at higher energies between 6 and 12 eV. The high energy resonance leads mainly to formation of H^-, but also to degradation of the ring structure. From the low energy contribution exclusively an abstraction of the neutral H atom occurs from the N-sites thereby forming the closed shell $[NB\text{-}H]^-$ anion. This hydrogen loss is remarkably site selective in thymine in that H abstraction at 1 eV proceeds only from N1 and at 1.8 eV only from N3.

Experiments in the gas phase allow a detailed characterisation of the intrinsic properties of a molecule and the dynamics of a particular reaction. Thereby the initial steps of electron induced strand breaks might be identified. For this it is essential to reveal the modifications of reactions and resonances, if a molecule is

coupled to other parts of the DNA.

2.2.3 Theoretical models

Based on the results of DEA to nucleobases theory proposed a transfer mechanism [20, 17], in which the excess charge initially localised on the nucleobase is transfered to the backbone. Calculations on the cytosine nucleotide predict a coupling of the π^* orbital of the nucleobase with a σ^* state of the sugar phosphate C-O bond. An electron that is captured by the base into the empty π^* orbital may thus cause a strand break between the sugar and phosphate group. However, the authors state that the rate of the reaction is rather low compared to autodetachment.

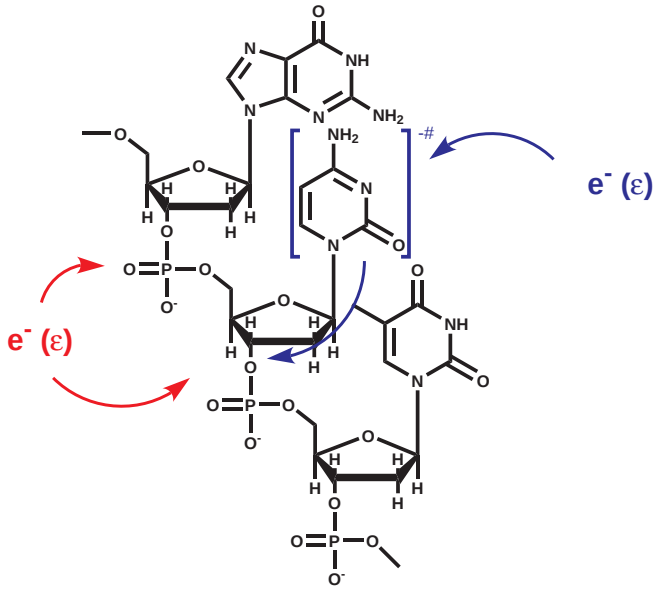

Figure 2.10: Part of a DNA single strand containing the nucleobases guanine, cytosine and thymine. A strand break occurs in the DNA backbone and may either be induced by low energy electron attachment to a nuclebase (blue) with subsequent transformation of the extra charge to the backbone (trnasfer mechanism), or alternatively by direct electron capture of the backbone (red).

On the other hand electron attachment to the backbone was considered to be operative already at very low energy. The investigation of vertical and adiabatic

potential surfaces for the thymidine phosphate anion [48] including solvation by water molecules and an Na^+ counter ion suggest that strand breaks may occur directly at the phosphate group.

Higher level calculations by other groups [49, 50] on nucleotides confirm that an electron can be captured close to zero eV, and is then localised on the base.

An alternative mechanism that includes only bound state anions [51] proposes that SSBs may be induced by proton transfer. For this a stable hydrogenated closed shell anion of a nucleobase (in the present example cytosine, Cy) is formed, for instance through electron induced hydrogen transfer followed by electron capture:

$$\mathrm{Cy...(HA)} + \mathrm{e^-} \rightarrow \mathrm{(CyH)^\bullet} + \mathrm{A^-} \xrightarrow{e^-} \mathrm{(CyH)^-} + \mathrm{A^-} \tag{2.25}$$

A subsequent intramolecular proton transfer from the sugar moiety to the nucleobase leads finally to a C-O bond cleavage. Due to the low barriers of the reactions and the fact that only bound anions contribute, the rates are much higher than in the transfer mechanism [51].

The experimental and theoretical results indicate that the fate of a negative charge localised on a particular part of DNA is still unresolved. Especially the role of the backbone is hardly explored and is therefore investigated in the present work.

2.3 Laser desorption techniques

In the present work a new instrument has been designed and constructed for the study of DEA to thermal labile biomolecules. These are transferred into the gas phase using laser induced acoustic desorption (LIAD). Furthermore DEA investigations of biomolecules are complemented by negative ion mass spectra obtained by matrix-assisted laser desorption and ionisation (MALDI). The basic principles of both techniques are presented in this section.

2.3.1 Laser induced acoustic desorption (LIAD)

Overview

A prerequisite to investigate DEA is the presence of neutral and intact biomolecules in the gas phase in order to ionise them afterwards in a controlled way by attachment of monoenergetic electrons. It was shown previously that laser induced acoustic desorption (LIAD) is a suitable means to desorb neutral fragile molecules without fragmentation [21, 52]. When the usefulness of laser generated stress waves for desorption of molecules had been revealed, the absence of ions was considered to be the main disadvantage in the application of this method [53, 52]. Consequently LIAD has been hardly applied in research, apart from the group of Kenttämaa, who advanced LIAD to study ion-molecule reactions in an FT-ICR spectrometer [21].
So far, LIAD has never been used in a beam experiment. First experiments, in which a LIAD source is combined with a low energy electron beam and a quadrupole mass spectrometer are presented in this work.

The desorption process in LIAD

In contrast to MALDI (see next session) the sample is not directly irradiated with the laser in LIAD. The molecules of interest are deposited on a thin titanium foil

(12.7 μm) that is irradiated from the backside with a pulsed laser.

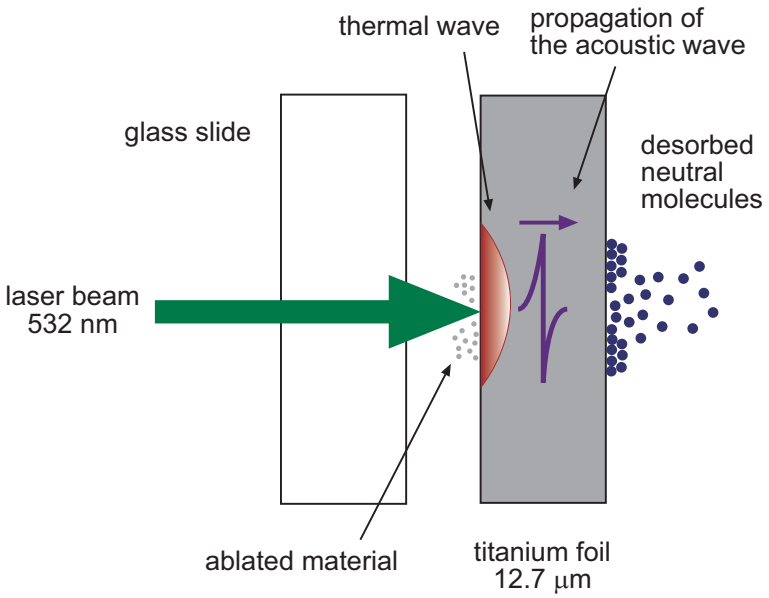

Figure 2.11: The desorption process in LIAD.

The light is focused on a small spot that heats the metal atoms in the direct vicinity of the spot with heating rates up to 10^{11} Ks^{-1} [54]. Due to thermal expansion in a very small volume a mechanical stress is caused that propagates into the bulk as an acoustic wave (Fig. 2.11). Additionally some metal is ablated from the surface and acoustic waves can be also a result from the recoil of ejected material. The acoustic pulse then reaches the opposite metal/gas interphase and gets reflected resulting in a distortion of the surface. Finally the analyte molecules are released without fragmentation and ionisation [53].

To efficiently create shock waves by laser irradiation the imparted energy must stay confined in the irradiated volume without being released by heat conduction. Hence the laser pulse duration should be below the thermal relaxation time τ_{th} that is given by [55, 56]:

$$\tau_{\mathrm{th}} = \frac{\rho \mathrm{c_p}}{4\lambda_{\mathrm{th}}}\delta^2 \tag{2.26}$$

with ρ being the density of the material (4.51×10^3 kgm^{-3} for Ti [57]), c_p the

specific heat ($0.523\,\mathrm{Jg^{-1}K^{-1}}$ [57]), δ the laser penetration depth and λ_{th} the thermal conductivity ($21.9\,\mathrm{Wm^{-1}K^{-1}}$ [57]). Assuming a penetration depth of $1\,\mu$m the thermal relaxation time becomes $\tau_{th} \approx 27\,$ns. That is the pulse length of the presently used laser (5 ns) is shorter than the thermal relaxation time making heat conduction less probable. This condition is termed "thermal confinement". Displacements caused in the material leads to the build-up of stress that can be released as acoustic wave within the acoustic relaxation time τ_{ac}, which is determined by the speed of sound v_s in the material:

$$\tau_{\mathrm{ac}} = \frac{\delta}{\mathrm{v_s}}. \tag{2.27}$$

For titanium this is 0.16 ns ($\mathrm{v}_s = 6070\,\mathrm{ms^{-1}}$ [57]), thus the energy of the laser pulse is released as an acoustic wave rather than by heat conduction if the laser pulse is short.

To ensure efficient generation of shock waves the metal that is used in LIAD should have a high thermal expansion coefficient, but also low thermal conductivity and low reflectivity for the laser wavelength. Different materials like copper, titanium, aluminum, gold, silver and iron have been tested for their suitability in LIAD [58] and Ti turned out to yield the best signal intensities. Despite a comparatively low thermal expansion coefficient of $11.9\times10^{-6}\,\mathrm{K^{-1}}$ [58] a production of acoustic waves is obviously favoured as Ti possesses the lowest reflectivity at 532 nm (0.50) of all investigated metals [58]. In other words, a large amount of energy is absorbed but only a small amount is conducted as a heat wave into the bulk material.

In previous experiments it was shown that the energy imparted into the molecules by the acoustic wave is not sufficient to ionise them. Thus only precharged ions have been observed with very low intensity [53]. In very recent experiments [59] it was estimated that the increase of internal energy of desorbed molecules is not more than a few $\mathrm{kcalmol^{-1}}$, i.e. below $\approx 400\,$meV.

2.3.2 Matrix assisted laser desorption/ionisation (MALDI)

MALDI is an ionisation technique that was developed in the 1980s [60, 61] and became a standard technique in mass spectrometry and analysis of biomolecules and polymers with a molecular weight of up to 10^6 Da.

The analyte is embedded in a matrix that is usually an aromatic organic acid (e.g. 2,5-dihydroxy-benzoic acid; 2,5 DBH) that possesses a chromophore absorbing light at the wavelength of the laser used. Upon irradiation with a laser - usually an N_2 laser (337 nm) in UV-MALDI - the matrix molecules are evaporated thereby carrying the analyte molecules into the gas phase. The laser pulse is short (usually a few ns) since rapid heating of a pure sample to high temperatures can preferentially lead to evaporation rather than decomposition of a thermal labile molecule [61].[2] If additionally a matrix is present that absorbs most of the laser light, sample molecules are transported predominantly intact into the gas phase. Both the desorption and ionisation processes are very complex and not fully understood to date [55], but it is established that for desorption a thermal mechanism dominates. The matrix serves also as a proton donor as well as acceptor in order to be able to ionise the sample molecules by protonation or deprotonation. The decomposition rate constant of the sample molecular ions and hence the fragmentation reaction can be fast, i.e. in the order of the phase transition process ("in-source-decay", ISD), or a slower unimolecular decay ("post-source-decay" PSD). Both processes are distinguished in experiments presented here.

[2] The rate constant for decomposition k_d is then higher than the rate constant for evaporation k_e due to a larger activation barrier E for evaporation according to the Arrhenius equation ($k = f \exp(-\frac{E}{kT})$). In an Arrhenius plot $\ln k = \ln f - E/kT$ the straight line lnk over 1/T is steeper for the evaporation reaction leading finally to preferred evaporation at high temperatures.